

# Failure in identification of overlapping spikes from multiple neuron activity causes artificial correlations

Izhar Bar-Gad <sup>a,\*</sup>, Ya'acov Ritov <sup>b</sup>, Eilon Vaadia <sup>a,c</sup>, Hagai Bergman <sup>a,c</sup>

<sup>a</sup> Center for Neural Computation, The Hebrew University, Jerusalem, Israel

<sup>b</sup> Department of Statistics, The Hebrew University, Jerusalem, Israel

<sup>c</sup> Department of Physiology, The Hebrew University, Hadassah Medical School, Jerusalem, Israel

Received 16 October 2000; received in revised form 26 January 2001; accepted 29 January 2001

## Abstract

Recording of multiple neurons from a single electrode is common practice during extra-cellular recordings. Separation and sorting of spikes originating from the different neurons can be performed either on-line or off-line using multiple methods for pattern matching. However, all spike sorting techniques fail either fully or partially in identifying spikes from multiple neurons when they overlap due to occurrence within a short time interval. This failure, that we termed the 'shadowing effect', causes the well-known phenomenon of decreased cross-correlation at zero offset. However, the shadowing effect also causes other artifacts in the auto and cross-correlation of the recorded neurons. These artifacts are significant mainly in brain areas with high firing rate or increased firing synchrony leading to a high probability of spike overlap. Cross correlation of cells recorded from the same electrodes tends to reflect the autocorrelation functions of the two cells, even when there are no functional interactions between the cells. Therefore, the cross-correlation function tends to have a short-term (about the length of the refractory period) peak. A long-term (hundreds of milliseconds to a few seconds) trough in the cross-correlation can be seen in cells with bursting and pausing activities recorded from the same electrode. Even the autocorrelation functions of the recorded neurons feature firing properties of other neurons recorded from the same electrode. Examples of these effects are given from our recordings in the globus pallidus of behaving primates and from the literature. Results of simulations of independent simple model neurons exhibit the same properties as the recorded neurons. The effect is analyzed and can be estimated to enable better evaluation of the underlying firing patterns and the actual synchronization of neighboring neurons recorded by a single electrode. © 2001 Elsevier Science B.V. All rights reserved.

**Keywords:** Cross-correlation; Spike sorting; Synchronization; Autocorrelation

## 1. Introduction

Extracellular recording of neuronal activity is a major tool in neurophysiological studies of the brain. Microelectrodes are used for recording local currents deriving from both spiking activity and local field potentials. A single electrode can potentially pick up signals from multiple cells within a local area (Abeles, 1974; Asanuma, 1989). Many types of studies of the nervous system function demand a separation of the recorded signal into spikes originating from different

cells. The spikes recorded from different neurons usually differ in size and shape, thereby enabling their sorting into the different sources (Lewicki, 1998; Harris et al., 2000). Recording and separation of multiple neurons from a single electrode allows examination of the behavior of a population of neurons that are usually much closer than multiple neurons recorded by different electrodes. Such studies are therefore mandatory for understanding local neural networks (Eggermont, 1990; Abeles, 1991).

There are plenty of methods for decomposing the output of single electrodes into parallel spike trains (see review of spike sorting methods in Lewicki, 1998). The methods differ in the algorithms used for sorting (ranging from amplitude discrimination to principal and

\* Corresponding author. Tel.: +972-2-6757388; fax: +972-2-6439736.

E-mail address: izharb@alice.nc.huji.ac.il (I. Bar-Gad).

independent component analysis of the spike shape), the working time frame (real time and offline methods) and the verification methods. In general, all methods suffer from problems common in classical signal detection methods, e.g. false positives (noise in the signal is classified as real spikes) and false negatives (real spikes are rejected as noise). However, when using spike-sorting methods, additional errors may occur. These errors include false match (a spike generated by one unit is classified to a different unit) and double match (a single waveform is classified as belonging to more than one class). The number of such errors can be reduced by better signal to noise recording conditions, and by more careful and elaborate sorting methods.

When the errors in either sorting or identification are systematic, they might cause effects, which seem to derive from the properties of the neurons rather than from the classification procedure (Quirk and Wilson, 1999). Such a systematic classification error occurs due to the spike overlap problem. All sorting methods perform quite well when the spikes recorded from the electrode are sufficiently separated in time. However, when multiple spikes appear closely, causing an overlap of their effects on the recorded signal, all sorting methods perform significantly worse. This overlap may result in several consequences: none of the spikes is identified (complete false negative); only one of the spikes is identified (partial false negative); or the overlapped signal is identified as another different spike (false match). The overlapping problem is usually not handled, although some methods have been developed for reducing the misidentification cause by the overlap (Lewicki, 1998). These methods include identification by neural networks (Chandra and Optican, 1997) and overlap decomposition (Atiya, 1992; Lewicki, 1994; Zouridakis and Tam, 1997). However, whichever methods are used, overlapping spikes are identified significantly worse than well-separated spikes. In this manuscript we show that the auto and cross-correlation functions of simultaneously recorded units (especially in brain areas with high firing rates and synchronized discharge) are significantly affected by the sorting limits. Thus, short and long term synchronization might appear in the cross-correlograms due to the sorting problems in spite of the fact that the neurons fire independently. Finally, we describe methods for estimating these artifacts, and thus enabling better understanding of the firing patterns and synchronization of neighboring neurons in the central nervous system.

## 2. Methods

### 2.1. Behavioral and recording methods

Real data was taken from electrophysiological

recordings of multiple spike trains from the globus pallidus of behaving monkeys. Details of the behavior of the monkeys and animal care are described elsewhere (Bar-Gad et al., 2000). During the recording sessions, eight glass-coated tungsten microelectrodes confined within a cylindrical guide (2.2 mm outer diameter) were advanced to the target. Neuronal activity from each electrode was amplified ( $\times 10\,000$ ), bandpass filtered (300–6000 Hz, four poles Butterworth filter, MCP 2.0 Alpha-Omega Engineering, Nazareth, Israel), and continuously sampled at 24 KHz/electrode (AlphaMap 4.8, Alpha-Omega Engineering). Detection and sorting of neural activity was done using real time and offline methods (see below). Only well-isolated and stable spike trains (as judged by stable spike waveforms, stable firing rate and consistent responses to behavioral events) were included in this study.

### 2.2. Real time spike sorting

The electrode output was sorted and classified in real time by a template-matching algorithm (MSD 3.21, Alpha-Omega Engineering). The electrode signal was continuously sampled at 50 KHz, placed in a buffer containing the last 100 samples (2 ms), and compared continuously with one to three templates. Each template was constructed of eight equally spaced points separated by 0.1 ms, and was defined by the user following a learning process of threshold crossing signals. The sum of squares of the differences between eight points in the buffer (starting 0.4 ms from the beginning of the buffer and equally spaced at 0.1 ms) and the templates was calculated. When this sum reached a minimum that was below a user-defined threshold, detection was hardware reported. In the cases that a buffer was double matched (e.g. a signal passed the criteria of more than one template), an error signal was given to the user, but no hardware report was created. A dead time of 0.06 ms followed detection. The timing of the hardware detections (100  $\mu$ s active low TTL pulses) were edge recorded at 12 KHz by a data logger (AlphaMap 4.8, Alpha-Omega Engineering) in parallel with the analog signals of the electrode output and of the behavioral events.

### 2.3. Offline spike sorting

The continuous (24 KHz) sampling of the electrode output was subject to off-line spike sorting procedure (AlphaSort 3.8, Alpha-Omega Engineering). This algorithm is based on principal component analysis of the spike pattern (Abeles and Goldstein, 1977). The algorithm assumes that most of the spike

waveform can be represented as a linear combination of two principal vectors, and that spikes generated by the same neurons will create a cluster of points in a two dimensional space representing the correlation between the spikes and the principal vectors. The principal vectors are calculated using existing libraries of extracellular recorded spikes in the relevant brain regions.

There are four steps in the off-line sorting procedure: extraction, projection, classification and, finally, verification. The first step is the extraction step, in which the program performs automatic detection of 2.7 ms segments with suspected spikes, based on threshold crossing. The threshold is calculated from the variance of the electrode output during the last 5.2 s. If more than one threshold crossing is detected in less than 1 ms, the higher one is selected. The candidate segments are extrapolated to 96 KHz, yielding 2.7 ms long segments with 256 sampling points. In the second step the suspected segments are projected on the two principal components and the approximation error of the original signal by the linear combination of the two principal vectors is calculated. To overcome the variability induced by the properties of the signal and the extraction step, the length of the principal vectors is 196 points ( $\sim 2$  ms) and the approximation error is calculated for all possible (60) offsets. The program finds the offset with the minimum approximation error and uses it for the classification step. In the classification step, the user is provided with a two dimensional display of all spikes with acceptable approximation error on the principal component space. The user classifies the neuron by drawing polygons around clusters of spike projections, and can subsequently modify these clusters along with the progression of the recording. Finally, the last and most critical step is the verification of the sorting. The user can test the waveforms of the sorted spikes, evaluate the stability of their shape and rate, their similarity to other sorted spikes and test their inter- and cross-spike interval histograms to be compatible with those of single neurons (Fee et al., 1996). The timing of the spikes is written at 12 KHz resolution, and all further analysis is performed using 1 ms bins.

The main advantages of the off-line sorting are that the user can make decisions with respect to the whole data. Decisions are not based only on current and recent past history. In addition, the user can re-evaluate those decisions using additional measures and statistical tests. Finally, off-line sorting reduces the sampling bias towards units with high firing rates, since a significant number of spikes can be accumulated over long recording even of cells with very low firing rates.

#### 2.4. Simulation techniques

Simplistic models of the neurons were used for simulating the shadowing effect. The spike trains of  $n$  mod-

eled cells were created as independent processes  $X_{1,t} \dots X_{n,t}$ . Each cell ( $m$ ), had a refractory period of length  $\tau_{\text{ref}}^m$  featuring lowered firing probability  $p_{\text{ref}}^m(t)$  followed by constant firing probability ( $p_{\text{const}}^m$ ). These cells are known as models of a Poisson process with a refractory period (MacGregor, 1987). The refractory period was defined for simplicity as an exponent function  $p_{\text{ref}}^m(t) = k^{(t/\tau_{\text{ref}}^m + 1 - t)} p_{\text{const}}^m$ ,  $t \leq \tau_{\text{ref}}^m$ ,  $k \leq 1$ . In addition, some of the cells featured long-term correlations in their firing rate. The long-term correlations were created by low probability ( $p_{\text{pause}}^m$ ) pauses of length  $t_{\text{pause}}^m$  in the cell's firing simulating the pauses typical to the external segment of the globus pallidus. The values for the variables used throughout the simulations were in accordance with those seen in the electrophysiological recordings of the globus pallidus  $4 \text{ ms} \leq \tau_{\text{ref}} \leq 10 \text{ ms}$ ,  $0.05 \leq p_{\text{const}} \leq 0.2$ ,  $500 \text{ ms} \leq t_{\text{pause}} \leq 3000 \text{ ms}$ ,  $10^{-4} \leq p_{\text{pause}} \leq 10^{-3}$  (DeLong, 1971).

Simulation of recording from a single electrode was performed for two different models: complete shadowing, removing all spikes of the two cells occurring within a single bin (Simple model) or partial shadowing, removal with different probabilities of spikes in temporally close occurrence (Complex model). The bins for the simulation were of the same length as those used for the electrophysiological recordings (1 ms). The length of the simulated processes was in the same order as the recorded data ( $10^6$  bins = 1000 s).

### 3. Results

#### 3.1. Electrophysiological recordings

Neurons recorded in the globus pallidus display common characteristics. The spontaneous firing rate of the cells is generally high compared to other brain areas (40–100 Hz), with a refractory period of several milliseconds (4–10 ms). The short time scale autocorrelation functions display a typical peak in the autocorrelation function following the refractory period (Fig. 1a,c). These peaks derive from the refractory period of the cells and not from an increased firing probability (Bar-Gad et al., 2000). The cross-correlation function between neurons recorded by different electrodes displays a flat correlogram in over 95% of neuron pairs (Nini et al., 1995; Raz et al., 2000) (Fig. 1d). However, the cross-correlation function of neurons recorded by the same electrode displays reduced probability around zero offset, followed by a short-term (narrow) peak. The duration of the short-term peak equals the duration of the refractory periods of the cells, and the peak is surrounded by short troughs in the correlation (Fig. 1b). Examples of cross-correlation functions of neurons recorded by the same electrode, featuring similar properties, appear in literature for

various brain regions: frontal cortex (Vaadia et al., 1991, Fig. 9d), dorsal cochlear nucleus (Voigt and Young, 1980, Fig. 9b), reticular formation region of the midbrain (MacGregor et al., 1975, Fig. 5b), medulla (Feldman et al., 1980, Fig. 7c), auditory cortex (Dickson and Gerstein, 1974, Figs. 5b,6j; Eggermont, 1992, Fig. 1a), substantia nigra (Wilson et al., 1977) and medial geniculate body (Heierli et al., 1987, Figs. 1,2).

The neurons of the globus pallidus (especially those of the external segment) display pausing activity (DeLong, 1971). The pauses reflect a decrease in firing rate from the typical high rate to very low rates for pro-

longed periods (500–3000 ms). This firing-pattern causes long-term (hundreds of milliseconds up to a few seconds) peaks in the autocorrelation functions (Fig. 2a-upper plot, c) (DeLong, 1971). Other cells may not display pausing activity, leading to a flat autocorrelation function (Fig. 2a-lower plot). The long-term cross-correlation between the neurons is flat when the cells are recorded by different electrodes (Fig. 2d). However, when the neurons are recorded by the same electrode, and at least one of the cells displays a long-term (wide) peak in the autocorrelation, the cross-correlation function reveals a typical long shallow trough of the same

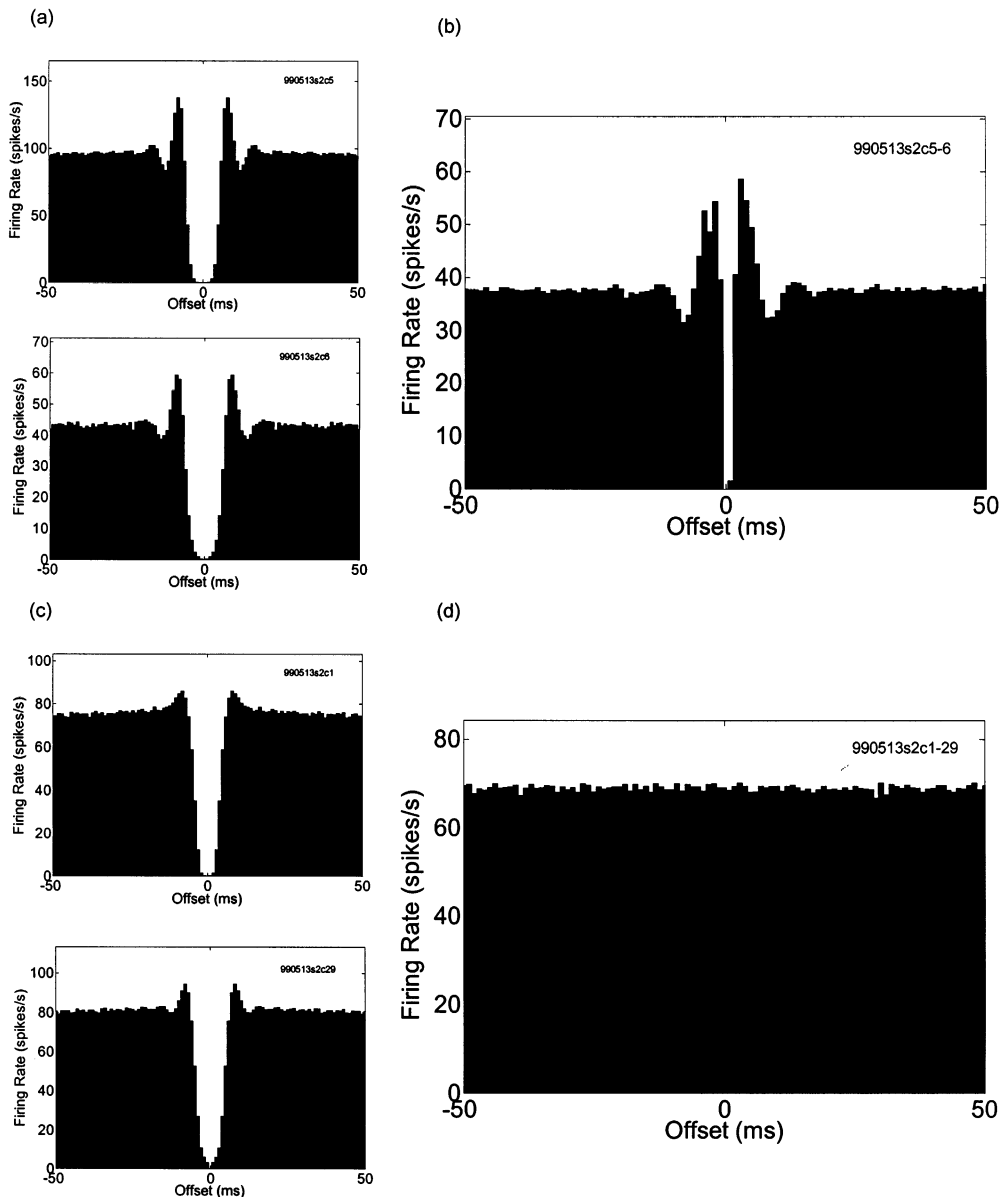


Fig. 1. Examples of short-term cross-correlation functions between neurons recorded from the same electrode and from different electrodes in the globus pallidus. (a) Autocorrelation functions of neurons recorded from a single electrode (990513/2/5 and 990513/2/6); (b) Cross-correlation function of the pair of neurons shown in (a), showing the typical short-term peak due to the shadowing effect; (c) Autocorrelation functions of neurons recorded from different electrodes (990513/2/1 and 990513/2/29); (d) Cross-correlation function of the pair of neurons shown in (c), showing the typical flat cross-correlation in the pallidum.

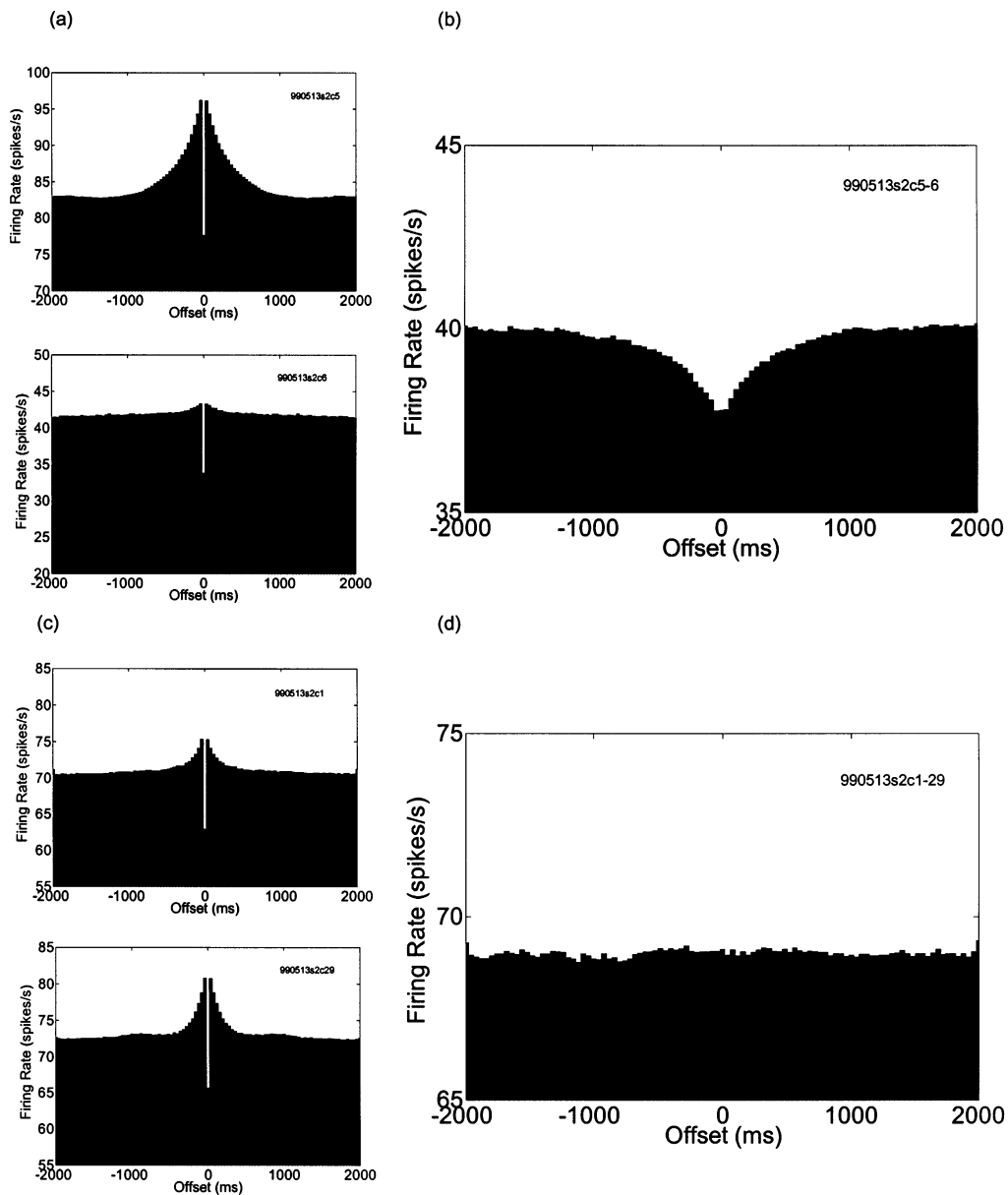


Fig. 2. Examples of long-term cross-correlation functions between neurons recorded from the same electrode and from different electrodes in the globus pallidus. (a) Autocorrelation functions of neurons recorded from a single electrode (990513/2/5 and 990513/2/6); (b) Cross-correlation function of the pair of neurons shown in (a), showing the typical long-term trough due to the shadowing effect; (c) Autocorrelation functions of neurons recorded from different electrodes (990513/2/1 and 990513/2/29); (d) Cross-correlation function of the pair of neurons shown in (c), showing the typical flat cross-correlation in the pallidum. In (a–d) 100 bins are displayed, each bin consists of the average of 40 ms. The bin-zero effects are therefore smoothed by the neighboring values.

time-scale as the peak in the autocorrelation function (Fig. 2b).

In general, when multiple neurons are recorded from the same electrode, their autocorrelation characteristics: oscillations, peaks and troughs tend to reflect onto the cross-correlation function. Prior research has shown that when cells are not independent i.e. have some functional connectivity, their cross-correlation function reflects their autocorrelation functions in various experimental setups (Eggermont, 1990). However, independent cells recorded from different electrodes do not

display this feature. In such cases the autocorrelation reflection is unique to recordings from the same electrode and is caused by the shadowing effect.

### 3.2. Simulations

Neurons were simulated independently with firing characteristics typical to those of the globus pallidus of primates. The simulated neurons featured a refractory period of decreased firing probability, followed by a period of constant firing probability. The combination

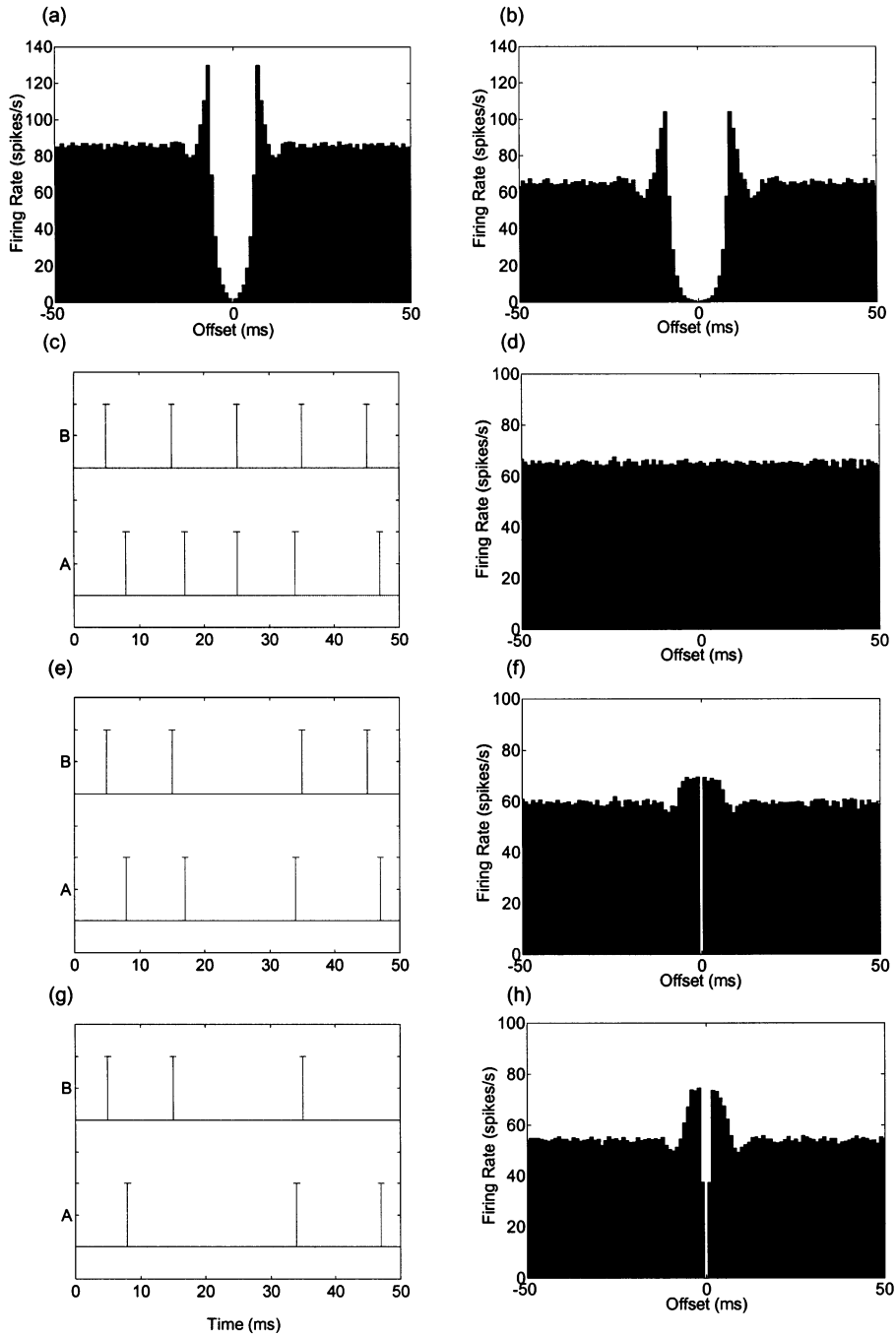


Fig. 3. Short-term cross-correlation: simulation results. (a–b) Autocorrelation of the two simulated independent cells before removal of common spikes; (c) Spike trains of two cells without removal of spikes occurring at the same bin, simulating recording from different electrodes; (d) Cross correlation of cells (a–b) without removal of spikes reveals a flat cross correlogram; (e) Spike trains of two cells after removal of spikes occurring at the same bin, simulating recording from the same electrode (simple shadowing); (f) Cross correlation cells (a–b) after removal of spikes occurring at the same bin reveals a small peak surrounding the zero valued central bin; (g) Spike trains of two cells after removal of spikes occurring at multiple bins, simulating recording from the same electrode (complex shadowing). Notice that in some cases spikes from both spike trains are removed, whereas at other times only one of the spike trains loses a spike; (h) Cross correlation of cells (a–b) after removal of spikes occurring at the multiple bins  $S_{m,n} = S_{n,m} = [0.5 \ 1 \ 0.5]$ , reveals a larger peak in the cross correlation function surrounding the three central bins. The parameters used in the figure are:

$$\Delta t = 1 \text{ ms}, \tau_1 = 6 \text{ ms}, p_1 = 0.15, \tau_2 = 8 \text{ ms}, p_2 = 0.12, p_t = k^{(\tau+1-t)} p \quad t \leq \tau, k = 0.5.$$

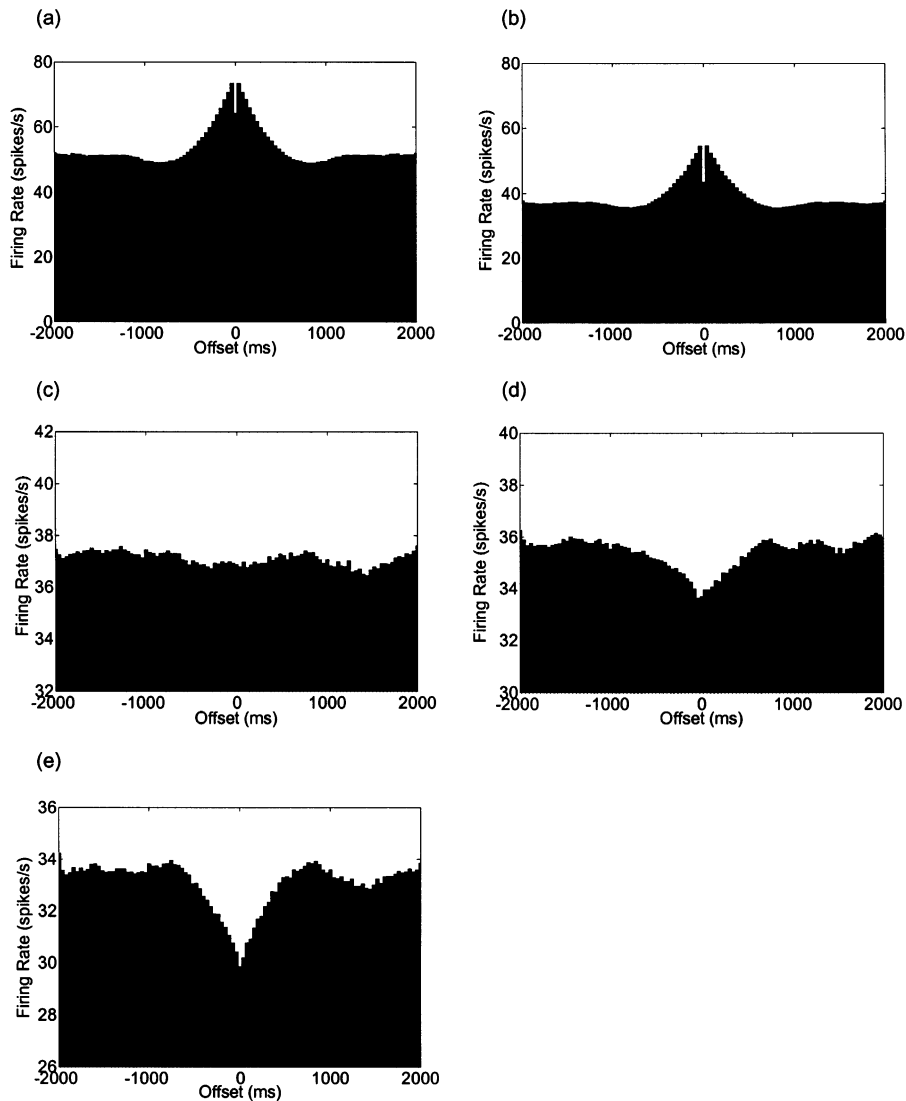


Fig. 4. Long-term cross correlation: simulation results. (a–b) Autocorrelation of the two cells before removal of common spikes; (c) Cross correlation of two simulated independent cells (a–b) without removal of spikes occurring at the same bin, simulating recording from different electrodes and demonstrating flat correlograms; (d) Cross correlation of two simulated independent cells (a–b) after removal of spikes occurring at the same bin, simulating recording from the same electrode and demonstrating a small trough in the correlogram; (e) Cross correlation of two simulated independent cells (a–b) after removal of spikes occurring at multiple bins  $S_{m,n} = S_{n,m} = [0.5 \ 1 \ 0.5]$  and demonstrating a large trough in the correlogram. The parameters used in the figure are:

$$\Delta t = 1 \text{ ms}, \tau_1 = 4 \text{ ms}, p_1 = 0.1, \tau_2 = 6 \text{ ms}, p_2 = 0.08, p_t = k^{(\tau+1-t)} p \quad t \leq \tau, k = 0.5. \quad p_{\text{pause}} = 0.001, \bar{t}_{\text{pause}} = 500 \text{ ms. Size of a bin is 40 ms.}$$

of high firing rate with the refractory period leads to autocorrelation functions with short peaks following the refractory period (Bar-Gad et al., 2000) (Fig. 3a,b). A short trace of spikes is shown for the two cells (Fig. 3c). Since the cells were created independently, the cross-correlation function is flat (Fig. 3d). However, a simple model simulating a recording of two cells by a single electrode can be obtained by removal of all spikes occurring within a single bin (Fig. 3e). The cross-correlation function created from the new spike trains (Fig. 3f) has the typical short-term peak seen in the experimental results. Creation of a more complex shadowing period

by removing common spikes for multiple offsets (e.g. in the range of  $\pm 2$  ms) with different probabilities (e.g. 100% at  $\pm 1$  ms and 50% at  $\pm 2$  ms, Fig. 3g) enhances the size of the peak in the cross-correlation (Fig. 3h).

To test the long-term shadowing effects we simulated independent neurons featuring a tendency towards pausing in the firing in addition to the refractory period properties. This firing pattern leads to a long-term peak in the autocorrelation functions in addition to the short-term phenomena (Fig. 4a,b). Since the cells are independent, their cross-correlation function is flat (Fig. 4c). However, the removal of spikes occurring in the

same bin causes the cross-correlation function to feature a wide trough (Fig. 4d) similar to the one seen in experimental data (Fig. 2b). This trough is also affected by the width of the shadowing effect and its shape, growing with the increase in the shadowing period length (Fig. 4e).

### 3.3. Analysis

For the analysis of the shadowing effect we shall first use the simple model of complete shadowing lasting for a single bin (removal of all common spikes within the central, zero offset, bin and no effect on spikes in any other bin). Another assumption is that only two cells are recorded from the same electrode. Both of these assumptions will be removed in the analysis of the general model. The details of the mathematical analysis are given in Appendix A.

Assuming that  $p_1$  and  $p_2$  are the firing probabilities of the original cells, before removal of common spikes. The firing probabilities of the two cells after removal of the common spikes equal the probability that one of the cells fired and the other did not.

$$p_n^* = p_n(1 - p_m), \quad (1)$$

where,  $n, m = 1, 2$ . Let:  $a_1(t)$  and  $a_2(t)$  be the autocorrelation functions of the original cells and assume independence of the underlying cells. The cross correlation of the two cells (at offset different than zero) after the removal of common spikes is given by,

$$c_{n,m}^*(t) = (1 - a_n(t))(1 - a_m(t)) \frac{p_n}{1 - p_n}. \quad (2)$$

The results of the analysis performed on the cells used for the simulation examples in the prior sections are similar to the computational (simulation) results.

The general model deals with a shadowing effect for multiple offset bins. The shadowing effect may not be complete, such that in each bin during the shadowing period ( $-\alpha$  to  $+\alpha$ ) the removal of spikes from cell  $m$  occurs with the probability  $S_{n,m}(t)$  where  $t$  is the offset from the spikes of cell  $n$ ,

$$\begin{aligned} 0 \leq S_{n,m}(t) \leq 1 & \quad |t| \leq \alpha. \\ S_{n,m}(t) = 0 & \quad |t| > \alpha \end{aligned} \quad (3)$$

The shadowing effect is not symmetric in time ( $S_{n,m}(t)$  is not necessarily equal to  $S_{n,m}(-t)$ ) and not symmetric between the neurons ( $S_{n,m}(t)$  is not necessarily equal to  $S_{m,n}(t)$  or  $S_{m,n}(-t)$ ). The firing probability in this case, under the assumption that the shadowing period is shorter than the refractory period, is

$$p_n^* = p_n \left( 1 - p_m \sum_{u=-\alpha}^{\alpha} S_{m,n}(u) \right). \quad (4)$$

The cross correlation of the two cells under the independence assumption is

$$\begin{aligned} c_{n,m}^*(t) = & \left( 1 - \sum_{u=-\alpha}^{\alpha} S_{n,m}(u) a_n(t+u) \right) \\ & \times \left( 1 - \sum_{u=-\alpha}^{\alpha} S_{n,m}(u) a_m(t-u) \right) \frac{p_n}{1 - p_n \sum_{u=-\alpha}^{\alpha} S_{n,m}(u)}. \end{aligned} \quad (5)$$

The equations describing the general solution are equal to the equations of the simple solution for  $\alpha = 0$ ,  $S_{n,m}(0) = S_{m,n}(0) = 1$ .

The size of the changes in the cross-correlation caused by the shadowing effect varies considerably according to the cells' characteristics such as firing probability and the shape of the autocorrelation function. The size of the change also varies according to features of the experimental setup and the sorting method that are reflected in the length and shape of the shadowing period. Assuming that the shadowing period is shorter than the absolute refractory period, the difference between the short-term peak in the cross correlation and the steady state can be approximated by,

$$\Delta c_{n,m}^* \approx p_n \left( p_n \sum_{u=-\alpha}^{\alpha} S_{n,m}(u) + p_m \sum_{u=-\alpha}^{\alpha} S_{m,n}(u) \right). \quad (6)$$

The size of the peak as a function of the firing rates, and of the shadowing period is shown (Fig. 5).

Assuming that the cells have a long-term peak in their autocorrelation functions (Fig. 2a,c and Fig. 4a,b), and that  $\Delta a_n$  and  $\Delta a_m$  are the maximum offsets of the peaks from steady state, the size of the trough in the cross correlation can be approximated by, (7)

$$\Delta c_{n,m}^* \approx -p_n \left( \Delta a_m \sum_{u=-\alpha}^{\alpha} S_{m,n}(u) + \Delta a_n \sum_{u=-\alpha}^{\alpha} S_{n,m}(u) \right).$$

Recording from a single electrode is not limited to two cells and may consist of multiple cells (Fig. 6). The shadowing effect is enhanced in such cases and is evident even in areas with slower firing rates. Even if some of the cells are not detected by the sorting devices, they may still bare an effect on the observed firing of the identified cells. Assuming that  $n$  neurons are recorded from the same electrode, the firing probability of any cell is affected by the other  $n-1$  neurons

$$p_i^{**} = p_i \prod_{k \neq i} \left( 1 - p_k \sum_{u=-\alpha}^{\alpha} S_{i,k}(u) \right). \quad (8)$$

The cross correlation of any two cells is

$$c_{i,j}^{**}(t) = c_{i,j}^*(t) \prod_{k \neq i,j} \left[ 1 - \frac{p_k}{1 - p_k \sum_{u=-\alpha}^{\alpha} S_{i,k}(u)} \right] \times \left( 1 - \sum_{u=-\alpha}^{\alpha} S_{i,k}(u) a_k(t+u) \right) \quad (9)$$

As before, the effects of the additional cells measured from the electrode can be significant depending on their firing rate and characteristics.

in the observed firing pattern of other neurons recorded by the same electrode in addition to the previously shown effects on their cross-correlation. This change in firing pattern may be evident in the autocorrelation function of the cell. The value of the autocorrelation function of a cell when two cells are recorded by the same electrode is for the simple case

$$a_n^*(t) = a_n(t) \left[ 1 - \frac{p_m}{1 - p_m} (1 - a_m(t)) \right], \quad (10)$$

and for the complex case

$$a_n^*(t) = a_n(t) \frac{1 - p_m \left[ 2 \sum_{u=-\alpha}^{\alpha} S_{m,n} + \sum_{u=-\alpha}^{\alpha} \sum_{v=-\alpha}^{\alpha} a_m(t-v+u) S_{m,n}(u) S_{m,n}(v) \right]}{1 - p_m \sum_{u=-\alpha}^{\alpha} S_{m,n}} \quad (11)$$

### 3.4. Autocorrelation effects

The firing pattern of one neuron may cause changes

The effect will usually be seen as a uniform decrease in the correlation function. However, although the effect is significantly smaller than the one reflected in the

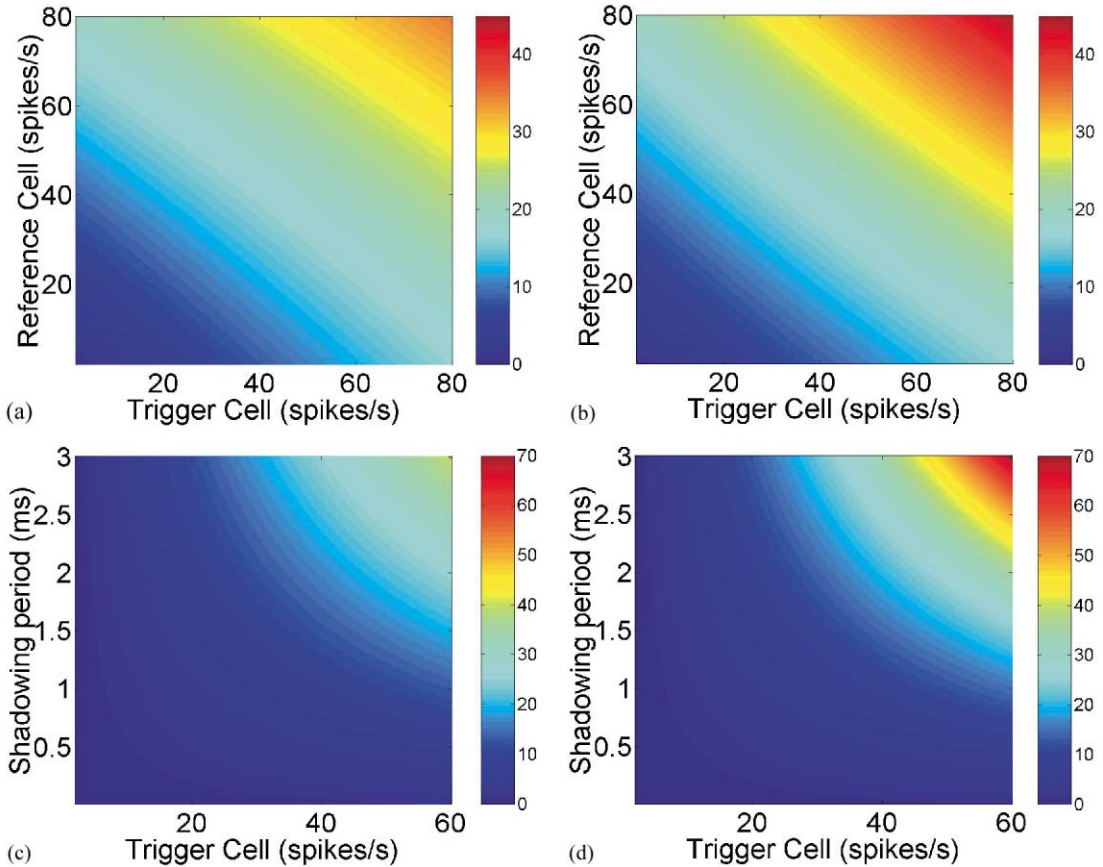


Fig. 5. Quantitative analysis of the size of the peak in the cross-correlation due to the shadowing effect. The size of the effect is reflected by the difference between the peak in the correlation and its steady state value and is color encoded showing the effect size normalized as a percent of the firing rate of the reference cell. (a) Assuming a 2 ms shadowing period and depending on the original firing rates; (b) Assuming a 2 ms shadowing period and depending on the observed firing rates. The relative effect is larger since the observed rate is equivalent to the higher original rate after removal of the shadowed spikes; (c) For various shadowing periods, assuming equal firing rates for both trigger and reference cells, depending on the original firing rates; (d) For various shadowing periods, assuming equal firing rates for both trigger and reference cells, depending on the observed firing rates.

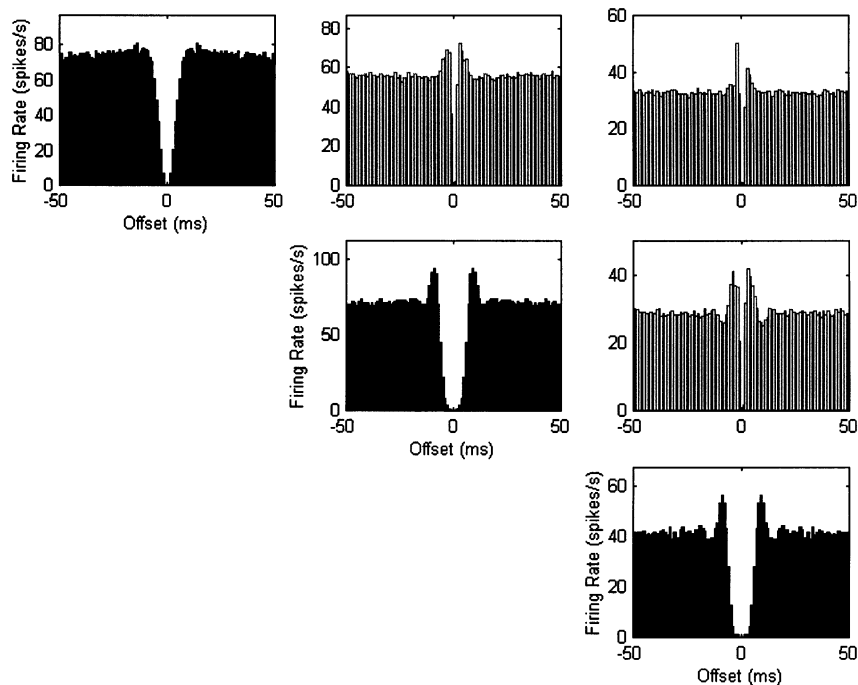


Fig. 6. Recording of multiple cells by the same electrode. (a) Autocorrelation and cross-correlation functions of three pallidal neurons recorded from the same electrode (990513/1/5, 990513/1/6 and 990513/1/7). Autocorrelation functions appear in filled bars and cross-correlation functions in empty bars.

cross-correlation, whenever one of the cells has a non-flat autocorrelation function such as an oscillatory activity, it changes the actual shape of the other autocorrelation function (Fig. 7).

#### 4. Discussion

The major points mentioned in the article are:

1. Cells recorded simultaneously from the same electrode and sorted using current sorting methods change each other's observed firing pattern. These changes in the auto and cross correlation functions are due to the 'shadowing effect'. This effect may exist even if a spike is not detected by the recording system.
2. The mutual effects of the cells are different, varying with the cells characteristics such as rate and shape of the original autocorrelation function, as well as parameters of the recording equipment such as the length and shape of the shadowing period.
3. The removal of the common spikes due to the shadowing effect causes changes in the correlation functions. The observed cross-correlation function reflects the inverted shape of the original autocorrelation functions (negative effect). The observed autocorrelation of a single cell features the shape of the autocorrelation of all the other cells recorded with it on the same electrode (positive effect).

The shadowing effect has different significance in different brain areas and during different recording paradigms. Generally, areas containing neurons with

high firing rates such as the basal ganglia and the cerebellum will have larger shadowing effects (Table 1). In addition to these areas that were simulated and analyzed throughout the article, areas with lower firing rates may also be affected when multiple cells in the local area tend to fire in synchrony. For example, cells in the cortex tend to fire at very low rates ( $< 5$  Hz). However, when activated, they may increase their rate significantly ( $> 100$  Hz). In many cortical areas neighboring cells tend to fire in synchrony during such activation (Gray et al., 1992). The co-activation may cause a severe shadowing problem during the increased firing periods and may therefore pose difficulties in drawing conclusions from the results regarding the local connectivity of neurons.

The shadowing effect may be significant even when the spike-sorting algorithm does not identify the cell causing it. A small amplitude spike with relatively small signal to noise ratio (SNR) may still cause additional false correlation between other cells recorded and identified by the same electrode. The effect can be estimated using formula Eq. (9), even if only a very general assumption can be made about the 'invisible cell'. Such is also the case with cells that have very small signal leading to partial detection of the spikes. This will lead to a significantly larger shadowing effect than is expected by the simple analysis derived from their visible firing. In addition to these physiological parameters, the experimental setup plays a key role: performance of online sorting will usually cause larger shadowing effects than off-line sorting due to reduced identification abilities.

Slower sampling systems of the analog waveform will also cause an increase in the shadowing effect, and so will simplified sorting methods and high noise levels. Furthermore, specific shadowing may affect a subset of the results: asymmetry in the shadowing effect is caused when one of the spikes is larger than the others, thereby shadowing them but remaining relatively unaffected by them. In addition, overlapping of two spikes may lead into an identification of a false third unit leading to false connectivity patterns.

Spike overlap has been a problem since the early days of multi-unit recording and spike sorting. Attempts to reduce the extent of the shadowing period have been performed by improving the signal to noise ratio and by creating overlap identification methods (Lewicki, 1998). However, after the sorting was completed, the shadowing period was generally ignored. Any subsequent analysis of the cross-correlation assumed that, except for the missing counts at offset zero, the cross-correlation functions of neighboring cells should be viewed as those recorded by different electrodes. Some studies quantitatively estimated the overlap effect by either examining the length of the short trough near zero ( $\pm 0.6$ – $2.0$  ms, Feldman et al., 1980) or by simulating the spike shapes and checking the expected overlap ( $\pm 0.8$ – $2.4$  ms of more

than 10% shadowing, Voigt and Young, 1980). In all these studies, the effects of the shadowing periods on the correlation at other time offsets were overlooked.

Clarification of the cross-correlation results and partial compensation for the shadowing effect can be achieved by estimating the size of the shadowing effects relevant for the brain area characteristics and the experimental setup. However, some other methods exist for reducing the effect and reducing its significance. Methods for improved recording such as usage of stereotrodes (McNaughton et al., 1983) and tetrodes (Harris et al., 2000) exist, enabling better potential separation of neighboring neurons. Further improvements can be performed during the spike identification and separation phases (Lewicki, 1998). However, all current methods do not overcome the shadowing effect completely leading to the need for awareness for the possibility of false phenomena derived from the systematic misidentification of overlapping spikes in multi-unit recording from a single electrode.

### Acknowledgements

This study was supported in part by the Israeli Academy of Science and the US-Israel Bi-national Sci-

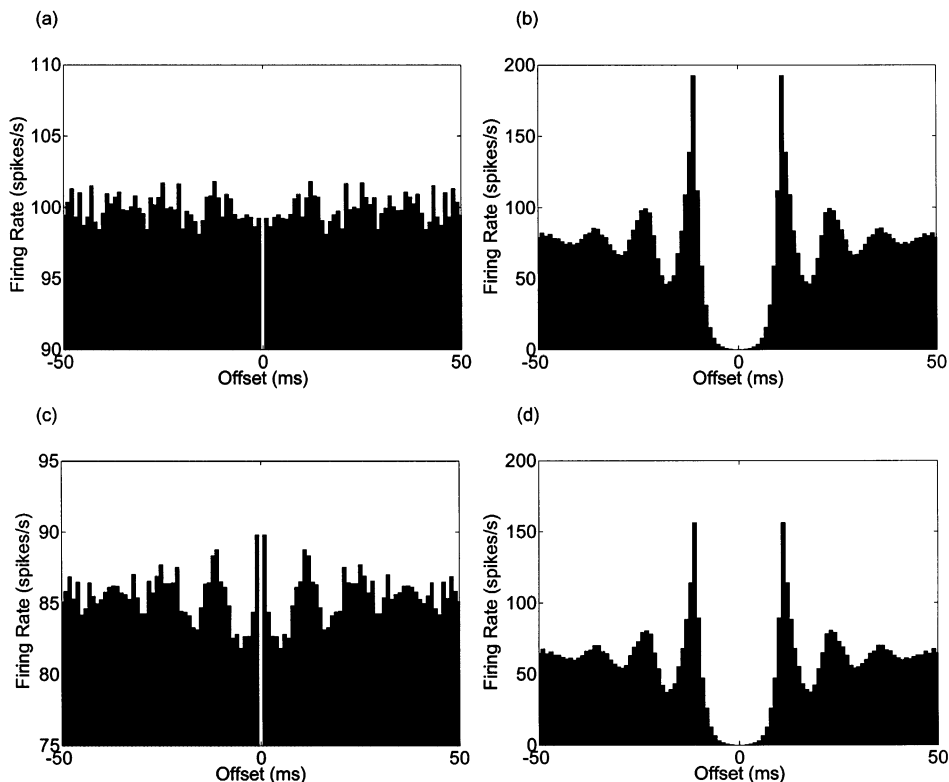


Fig. 7. Mutual effects of the autocorrelation functions. (a) Autocorrelation function of a simulated cell with a Poisson firing pattern. (b) Autocorrelation function of a simulated cell with 80 Hz noisy oscillation. (c) Autocorrelation of the cell shown in (a) after removal of common spikes with (b), showing the reflection of the oscillatory 'neighbor' (Y-scale in A and C is adjusted to the correlation level to show the emerged oscillatory phenomena). (d) Autocorrelation of the cell shown in (b) after removal of common spikes with (a). The removal of the spikes simulated a complex shadowing period of the form  $S_{m,n} = S_{n,m} = [0.5 \ 1 \ 0.5]$ .

Table 1  
Typical values for the cross-correlation short-term peak for different brain areas<sup>a</sup>

	Observed firing rate (spikes/s)	Original firing rate (spikes/s)	$\Delta p$	$\Delta p/p$ (%)
<i>Online sorting values <math>\alpha = 2</math>,</i> $S_{m,n} = S_{n,m} = [0.25 \ 0.75 \ 1 \ 0.75 \ 0.25]$				
Globus Pallidus	60	78.5	42.6	71.1
STN	25	27.2	4.6	18.6
Cortex	5	5.1	0.2	3.1
<i>Offline sorting values <math>\alpha = 1</math>,</i> $S_{m,n} = S_{n,m} = [0.5 \ 1 \ 0.5]$				
Globus Pallidus	60	69.7	21.0	35.0
STN	25	26.4	2.9	11.5
Cortex	5	5.1	0.1	2.1

<sup>a</sup> The size of the shadowing effect differs according to the characteristics of the brain area and of the experimental setup for the spike detection process. The size of the effect is given in the table for various regions assuming two typical experimental setups.

ence Foundation. We thank Moshe Abeles, Yoram Ben-Shaul and Genella Morris for their critical reading and helpful suggestions. We thank Gali Havazelet-Heimer, Joshua A. Goldberg and Sharon Maraton for sharing their data with us.

## Appendix A

The cells can be described as independent stationary (0, 1) processes  $X_{n,t}$  where  $n$  indicated the process number and  $t$  the time. A value of 1 of the process is equivalent to a spike for the simulated cell. The firing probability of the original process  $X_n$  is

$$p_n = P(X_{n,t} = 1), \quad (\text{A1})$$

and the autocorrelation function of the processes is

$$a_n(t) = P(X_{n,t} = 1 | X_{n,0} = 1). \quad (\text{A2})$$

The cross correlation function of the cells when independence is assumed is flat

$$c_{n,m}(t) = P(X_{n,t} = 1 | X_{m,0} = 1) = p_n. \quad (\text{A3})$$

For the analysis of the removal of common spikes we first assume a simple case of a complete shadowing effect lasting a single bin. Another assumption that is made for simplicity is that only two cells are recorded from the same electrode. Both of these assumptions are removed in the analysis of the general case. The firing probabilities of the two cells after removal of the common spikes is

$$p_n^* = P(X_{n,t}^* = 1) = P(X_{n,t} = 1, X_{m,t} = 0) = p_n(1 - p_m). \quad (\text{A4})$$

The cross correlation of the two cells is

$$\begin{aligned} c_{n,m}^*(t) &= P(X_{n,t}^* = 1 | X_{m,0}^* = 1) \\ &= \frac{P(X_{n,t} = 1, X_{n,0} = 0, X_{m,0} = 1)}{P(X_{m,0} = 1, X_{n,0} = 0)} \end{aligned} \quad (\text{A5})$$

$$= (1 - a_n(t))(1 - a_m(t)) \frac{p_n}{1 - p_n}.$$

and the autocorrelation is

$$\begin{aligned} a_n^*(t) &= P(X_{n,t}^* = 1 | X_{n,0}^* = 1) \\ &= \frac{P(X_{n,t} = 1, X_{n,0} = 1, X_{m,t} = 0, X_{m,0} = 0)}{P(X_{n,0} = 1, X_{m,0} = 0)} \\ &= a_n(t) \left[ 1 - \frac{p_m}{1 - p_m} (1 - a_m(t)) \right]. \end{aligned} \quad (\text{A6})$$

Recording from a single electrode is not limited to two cells and might consist of multiple cells. The shadowing effect is enhanced in such a case and is evident even in areas with slower firing rate. The formulation for the simple case (shadowing of a single bin) follows the same lines used for two cells. Assuming that  $n$  independent processes  $X_{1,t}, \dots, X_{n,t}$  simulate the cells, the firing probability is

$$\begin{aligned} p_i^* &= P(X_{i,t}^* = 1) = P(X_{i,t} = 1, X_{k \neq i,t} = 0) \\ &= p_i \prod_{k \neq i} (1 - p_k). \end{aligned} \quad (\text{A7})$$

The cross correlation of two cells is

$$\begin{aligned} c_{i,j}^*(t) &= P(X_{i,t}^* = 1 | X_{j,0}^* = 1) \\ &= \frac{P(X_{i,t} = 1, X_{k \neq i,t} = 0, X_{j,0} = 1, X_{k \neq j,0} = 0)}{P(X_{j,0} = 1, X_{k \neq j,0} = 0)} \\ &= (1 - a_i(t))(1 - a_j(t)) \\ &\quad \frac{p_i}{1 - p_i} \prod_{k \neq i,j} \left[ 1 - \frac{p_k}{1 - p_k} (1 - a_k(t)) \right], \end{aligned} \quad (\text{A8})$$

and the autocorrelation function values are

$$\begin{aligned} a_i^*(t) &= P(X_{i,t}^* = 1 | X_{i,0}^* = 1) \\ &= \frac{P(X_{i,t} = 1, X_{i,0} = 1, X_{k \neq i,t} = 0, X_{k \neq i,0} = 0)}{P(X_{i,0} = 1, X_{k \neq i,0} = 0)} \\ &= a_i(t) \prod_{k \neq i} \left[ 1 - \frac{p_k}{1 - p_k} (1 - a_k(t)) \right]. \end{aligned} \quad (\text{A9})$$

The complex shadowing period that enables description of the general misidentification effects can be described by the probabilities of the misidentification  $S_{n,m}(t)$  of neuron  $m$  caused by neuron  $n$  at offset  $t$ . An auxiliary variable that is important is the sum of these effects:

$$T_{n,m} = p_n \sum_{u=-\alpha}^{\alpha} S_{n,m}(u). \quad (\text{A10})$$

The firing probability for the general case can be described as

$$\begin{aligned} p_n^* &= P(X_{n,0}^* = 1) = P(X_{n,0} = 1) - P(X_{n,0} = 1, X_{n,0}^* = 0) \\ &= p_n - p_n p_m \sum_{u=-\alpha}^{\alpha} S_{m,n} = p_n (1 - T_{m,n}). \end{aligned} \quad (\text{A11})$$

The cross-correlation of two neurons is

$$\begin{aligned} c_{n,m}(t) &= P(X_{n,t}^* = 1 | X_{m,0}^* = 1) \\ &= \frac{P(X_{n,t} = 1, X_{m,0} = 1) P(X_{n,t}^* = 1 | X_{n,t} = 1, X_{m,0} = 1) P(X_{m,0}^* = 1 | X_{n,t} = 1, X_{m,0} = 1)}{P(X_{m,0} = 1)} \\ &= \frac{p_m}{1 - T_{m,n}} \left( 1 - \sum_{u=-\alpha}^{\alpha} a_m(t+u) S_{m,n}(u) \right) \left( 1 - \sum_{u=-\alpha}^{\alpha} a_n(t-u) S_{m,n}(u) \right) \end{aligned} \quad (\text{A12})$$

The autocorrelation is,

$$\begin{aligned} a_n^*(t) &= P(X_{n,t}^* = 1 | X_{n,0}^* = 1) \\ &= \frac{P(X_{n,t} = 1, X_{n,0} = 1) P(X_{n,t}^* = 1, X_{n,0}^* = 1 | X_{n,t} = 1, X_{n,0} = 1)}{P(X_{n,0} = 1)}, \\ &= a_n(t) \frac{1 - p_m \left[ 2 \sum_{u=-\alpha}^{\alpha} S_{m,n} + \sum_{u=-\alpha}^{\alpha} \sum_{v=-\alpha}^{\alpha} a_m(t-v+u) S_{m,n}(u) S_{m,n}(v) \right]}{1 - p_m \sum_{u=-\alpha}^{\alpha} S_{m,n}} \end{aligned}$$

## References

- Abeles M. A journey into the brain. In: Inbar GF, editor. Signal Analysis and Pattern Recognition in Biomedical Engineering. New-York: John Wiley & Sons, 1974:41–59.
- Abeles M. Corticonics — Neural Circuits of the Cerebral Cortex. Cambridge: Cambridge University Press, 1991.
- Abeles M, Goldstein MHJ. Multispike train analysis. IEEE Trans Biomed Eng 1977;65:762–73.
- Asanuma H. The Motor Cortex. New-York: Raven Press, 1989:1–189.
- Atiya AF. Recognition of multiunit neural signals. IEEE Trans Biomed Eng 1992;39:723–9.
- Bar-Gad I, Ritov Y, Bergman H. The neuronal refractory period causes a short-term peak in the autocorrelation function. J. Neurosci. Methods. 2000;104:155–63
- Chandra R, Optican LM. Detection, classification, and superposition resolution of action potentials in multiunit single-channel recordings by an on-line real-time neural network. IEEE Trans Biomed Eng 1997;44:403–12.
- DeLong MR. Activity of pallidal neurons during movement. J Neurophysiol 1971;34:414–27.
- Dickson JW, Gerstein GL. Interactions between neurons in auditory cortex of the cat. J Neurophysiol 1974;37:1239–61.
- Eggermont JJ. The Correlative Brain. Theory and Experiment in Neuronal Interaction. Berlin: Springer-Verlag, 1990.
- Eggermont JJ. Neural interaction in cat primary auditory cortex. Dependence on recording depth, electrode separation, and age. J Neurophysiol 1992;68:1216–28.

- Fee MS, Mitra PP, Kleinfeld D. Variability of extracellular spike waveforms of cortical neurons. J Neurophysiol 1996;76:3823–33.
- Feldman JL, Sommer D, Cohen MI. Short time scale correlations between discharges of medullary respiratory neurons. J Neurophysiol 1980;43:1284–95.
- Gray CM, Engel AK, Konig P, Singer W. Synchronization of oscillatory neuronal responses in cat striate cortex: temporal properties. Vis Neurosci 1992;8:337–47.
- Harris KD, Henze DA, Csicsvari J, Hirase H, Buzsaki G. Accuracy of tetrode spike separation as determined by simultaneous intracellular and extracellular measurements. J Neurophysiol 2000;84:401–14.
- Heierli P, de-Ribaupierre F, de-Ribaupierre Y. Functional properties and interactions of neuron pairs simultaneously recorded in the medial geniculate body of the cat. Hear Res 1987;25:209–25.
- Lewicki MS. Bayesian modeling and classification of neural signals. Neural Comp 1994;6:1005–30.
- Lewicki MS. A review of methods for spike sorting: the detection and classification of neural action potentials. Network 1998;9:R53–78.

- MacGregor RJ. Neural and Brain Modeling. San-Diego: Academic Press Inc., 1987.
- MacGregor RJ, Miller SW, Groves PM. Slow rhythms and correlations in spike trains from midbrain neurons. Exp Neurol 1975;47:581–98.
- McNaughton BL, O'Keefe J, Barnes CA. The stereotrode: a new technique for simultaneous isolation of several single units in the central nervous system from multiple unit records. J Neurosci Methods 1983;8:391–7.
- Nini A, Feingold A, Slovov H, Bergman H. Neurons in the globus pallidus do not show correlated activity in the normal monkey, but phase-locked oscillations appear in the MPTP model of parkinsonism. J Neurophysiol 1995;74:1800–5.
- Quirk MC, Wilson MA. Interaction between spike waveform classification and temporal sequence detection. J Neurosci Methods 1999;94:41–52.
- Raz A, Vaadia E, Bergman H. Firing pattern and correlations of spontaneous discharge of pallidal neurons in the normal and the tremulous MPTP vervet model of parkinsonism J Neurosci 2000; In press.
- Vaadia E, Ahissar E, Bergman H, Lavner Y. Correlated activity of neurons: a neural code for higher brain functions? In: Kruger J, editor. Neuronal Cooperativity. Berlin: Springer-Verlag, 1991:249–79.
- Voigt HF, Young ED. Evidence of inhibitory interactions between neurons in dorsal cochlear nucleus. J Neurophysiol 1980;44:76–96.
- Wilson CJ, Young SJ, Groves PM. Statistical properties of neuronal spike trains in the substantia nigra: cell types and their interactions. Brain Res 1977;136:243–60.
- Zouridakis G, Tam DC. Multi-unit spike discrimination using wavelet transforms. Comput Biol Med 1997;27:9–18.